Electrocatalysis

Deutsche Ausgabe: DOI: 10.1002/ange.201509593
Internationale Ausgabe: DOI: 10.1002/anie.201509593

Electrocatalytic O_2 Reduction at a Bio-inspired Mononuclear Copper Phenolato Complex Immobilized on a Carbon Nanotube Electrode

Solène Gentil[+], Doti Serre[+], Christian Philouze, Michael Holzinger, Fabrice Thomas, and Alan Le Goff**

Abstract: *An original copper-phenolate complex, mimicking the active center of galactose oxidase, featuring a pyrene group was synthesized. Supramolecular pi-stacking allows its efficient and soft immobilization at the surface of a Multi-Walled Carbon Nanotube (MWCNT) electrode. This MWCNT-supported galactose oxidase model exhibits a $4H^+/4e^-$ electrocatalytic activity towards oxygen reduction at a redox potential of 0.60 V vs. RHE at pH 5.*

The design of electrocatalysts for the oxygen reduction reaction (ORR) currently drives a considerable interest. This stems from the increasing demand for new cathodic electrode materials employing non-noble metals for application in fuel cell technologies, which overcome slow kinetics inherent to the complete $4H^+/4e^-$ oxygen reduction to water. In nature, dioxygen reduction is managed by copper metalloenzymes,[1–3] which then represent a formidable challenge for chemists to emulate.[4–8] This reaction is involved in the oxidation of alcoholic substrates of the copper oxidases. In these enzymes the copper ion only shuttles between its Cu(II) and Cu(I) oxidation states during turnovers because trivalent copper is not thermodynamically accessible under biological conditions. Consequently, the number of copper atoms present in the protein often matches the number of electrons involved in dioxygen reduction.[2] Perhaps the most representative examples are catechol oxidase and laccases, which perform the two-electron reduction of dioxygen at a binuclear active site and four-electron reduction of dioxygen by using a $3+1$ arrangement of copper centers, respectively. Galactose oxidase is a particular case of a two-electron reduction of dioxygen at a mononuclear copper site. This paradox is explained by the involvement of an additional redox center in the reaction, which was identified as a tyrosyl radical (phenoxyl/phenolato redox couple).[9]

When an efficient immobilization and direct wiring of copper oxidases are achieved at the surface of an electrode, these enzymes have demonstrated low overpotentials of only several tens of millivolts and high current densities towards $4H^+/4e^-$ oxygen reduction.[10–12] The efficient wiring of galactose oxidase has also demonstrated its activity towards oxygen electroreduction.[13] Owing to a direct electron transfer between gold electrode and the enzyme active site, the ORR activity of immobilized galactose oxidase was displayed at the redox potential of the Cu^{II}/Cu^{I} redox center, that is, 70 mV versus Ag/AgCl at pH 7.5.

When dealing with the immobilization of molecular catalysts and enzymes for electrocatalytic applications, carbon nanotubes (CNTs) combine many advantages: i) high efficiency towards the flexible and stable immobilization of a high amount of catalysts per surface unit; ii) superior heterogeneous electron transfer properties; and iii) the availability of a library of non-covalent and covalent functionalization techniques. We and others have investigated the pi–pi interactions of pyrene-modified molecular electrocatalysts for proton reduction,[14] CO_2 reduction,[15,16] or NADH oxidation.[17] Owing to their high stability, pyrene groups can be easily introduced during synthesis. Additionally, pyrene pi-stacking provides a soft and controllable functionalization technique of CNT sidewalls that prevents CNT damages and conductivity losses.

Herein, we describe the preparation of a copper phenolato complex bearing a pyrene group (**1**) and its efficient supramolecular immobilization on CNTs. We observe ORR activity of this CNT-supported galactose oxidase model.

The tripodal ligand **LH** was prepared by reductive amination of the aldehyde precursor ^{CHO}**LH** (Supporting Information) with N^1-(pyren-1-ylmethyl)butane-1,4-diamine (PBDI; Scheme 1).[18] **LH** reacted with one molar equivalent

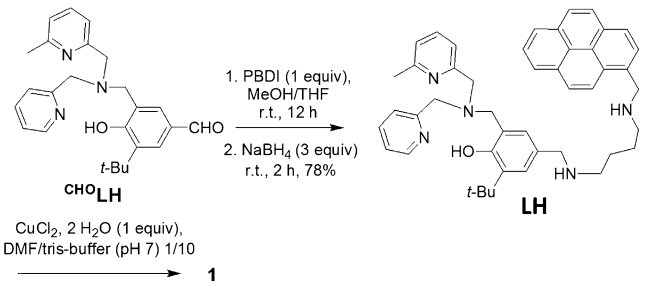

Scheme 1. Simplified synthetic procedure leading to **LH** and **1**.

of $CuCl_2$, $2H_2O$ in water to give complex **1**. The structure of **1** in aqueous solution was established by EPR and UV/Vis spectroscopy (Supporting Information, Figures S1–S4 and Table S1). The X-band EPR spectrum of **1** in a DMF/tris-

[*] S. Gentil,[+] D. Serre,[+] Dr. C. Philouze, Dr. M. Holzinger, Prof. F. Thomas, Dr. A. Le Goff
Département de Chimie Moléculaire, UMR CNRS 5250
Univ. Grenoble Alpes
570 rue de la Chimie, B. P. 53, 38041 Grenoble cedex 9 (France)
E-mail: alan.le-goff@ujf-grenoble.fr
fabrice.thomas@ujf-grenoble.fr
[+] These authors contributed equally to this work.

Supporting information and ORCID(s) from the author(s) for this article are available on the WWW under http://dx.doi.org/10.1002/anie.201509593.

 © 2016 Wiley-VCH Verlag GmbH & Co. KGaA, Weinheim

buffer (pH 7) 1:9 solution consists of a well-resolved axial ($S = {}^1/_2$) copper(II) signal (Figure S3), authenticating a mononuclear copper species. Further, the g values ($g_\parallel = 2.248$ and $g_\perp = 2.051$) are consistent with a distorted square pyramidal environment of the copper ion. The electronic spectrum of **1** at pH 7 displays a main band at 457 nm ($\varepsilon = 1150\,\text{M}^{-1}\,\text{cm}^{-1}$), which is assigned to a phenolato-to-copper charge transfer (CT) transition. The CT band disappears upon decreasing the pH, consistent with the protonation of the phenolate group (Figure S4). The pK_a was determined from spectrophotometric titration at 3.93 ± 0.02 in a DMF/H_2O 1:9 solution. Owing to the electron-donating properties of the phenolate substituent, this value appears remarkably low. This indicates that the phenolate is bound to the metal, which is a strong Lewis acid, and occupies a weakly labile, that is, equatorial, position in the coordination polyhedron. Since **1** could not be isolated as single crystals for an X-ray diffraction study, most likely owing to the hygroscopic nature and the flexibility of the pyrene-putrescine arm, we prepared the copper complex of its precursor $^{\text{CHO}}$**LH**, namely **2** (Figures S5–7). The crystal structure of **2** (Figure S6) confirms that the metal ion lies in a square pyramidal geometry, with the sterically hindered α-methylpyridine coordinated in the axial position (Cu–N bond at 2.303(2) Å). The phenolate is tightly bound in equatorial position (with a Cu–O bond distance of 1.919(2) Å), along with the pyridine, tertiary amine, and a chloride anion.

The design of functionalized MWCNT electrodes is based on successive incubation steps. The first incubation step is driven by the pi–pi interactions of **LH** (3 mM in acetonitrile) with the MWCNT film surface. The second incubation step is driven by the high affinity of immobilized **LH** towards copper(II) (0.3 mM $CuCl_2$ in ultrapure water; Figure 1 A).

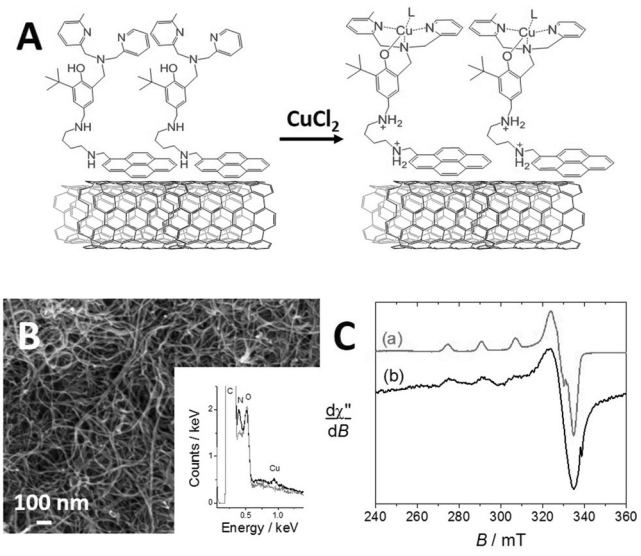

Figure 1. A) Representation of the synthesis of complex **1** starting from LH on MWCNT; B) SEM image of the surface of the functionalized MWCNT electrode (inset : EDX analysis); C) 100 K EPR spectra of a) **1** in 0.5 mM water:DMF (90:10) solution (pH 4.99) and b) Difference between a functionalized MWCNT electrode and MWCNT (microwave freq. 9.46 GHz, power : a) 4.4 or b) 5.5 mW, mod. amp. a) 0.4 and b) 0.5 mT, mod. freq. 100 kHz).

The functionalized MWCNT electrodes were characterized by SEM, EDX, and solid-state EPR (Figure 1 B and C). SEM images confirm the high specific surface of the MWCNT film. The comparative EDX analysis between pristine and functionalized MWCNTs confirms the presence of copper and nitrogen on the surface of MWCNTs with a ratio N/Cu ≈ 4, arising from the presence of both the ligand **LH** and the copper center, with a complex **1** formation yield of ≈ 80 %. Carbon and oxygen mostly originate from the MWCNTs (inset, Figure 1 B). Furthermore, the solid-state EPR spectrum of functionalized MWCNTs exhibits a typical copper(II) signal (Figure 1 C), which is not present in pristine MWCNTs. The copper hyperfine splitting is clearly visible, indicating that the complexes are magnetically isolated on the MWCNT surface. It is significant that the hyperfine splitting differs from that expected for free copper. Conversely, it is close to that observed for **1** in a DMF/H_2O solution, confirming that the complex retains its integrity on CNT sidewalls. The cyclic voltammetry (CV) curve of the functionalized electrode was performed in aqueous medium (Figure 2).

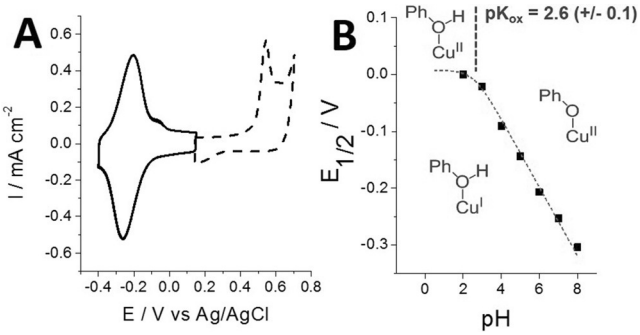

Figure 2. A) CVs of complex **1** immobilized on the MWCNT electrode in 0.1 M $LiClO_4$ ($v = 10\,\text{mV s}^{-1}$) under argon; B) Experimental (squares) and fitted (dashed line) evolution of the redox potential of the Cu^{II}/Cu^{I} redox couple as a function of the pH in 0.1 M Britton–Robinson buffer between pH 2 and 8. The geometrical surface of the electrode ($0.07\,\text{cm}^{-2}$) was taken to calculate current densities.

Under anaerobic conditions, the CV of the MWCNT-supported complex **1** displays a well-defined reversible redox system at $E_{1/2} = -0.24$ V (pH 7, reference Ag/AgCl), assigned to the Cu^{II}/Cu^{I} redox couple (Figure 2 A). The oxidation of the phenolate into a phenoxyl radical is irreversible and occurs at $E_p^a = 0.55$ V.[19] Both anodic and cathodic peak currents increase linearly with increasing scan rates, confirming the stable immobilization of **1** on MWCNT electrodes (Figure S8A and B). By integration of the cathodic peak, a maximum surface coverage of $\Gamma_1 = 0.42\,\text{nmol cm}^{-2}$ was estimated. The ΔE_p of 40 mV at slow scan rate increases with increasing scan rates. By using the Laviron equation for immobilized redox systems,[20] the apparent heterogeneous electron transfer rate k_0^{app} of $0.45\,\text{s}^{-1}$ was determined (Figure S8C). This relatively low value is consistent with previously measured k_0 values for other surface-confined copper complexes, and is likely caused by an electrochemically induced structural rearrangement of the copper coordination

 © 2016 Wiley-VCH Verlag GmbH & Co. KGaA, Weinheim

sphere.[7] Further, the study of this redox system over a broad pH range (Figure 2B) revealed a decrease in $E_{1/2}$ with increasing pH, which was fitted according to Equation (1):

$$E_{1/2} = E_{1/2}(Cu^{II/I}{}_{acid}) + \frac{2.3RT}{nF}\log\left(1+\frac{[K_a]}{[H^+]}\right) \quad (1)$$

Where R is the gas constant, T the temperature, F the Faraday constant, and n the number of electron involved in the redox system. K_a is the proton dissociation constant for complex **1** and $E_{1/2}(Cu^{II/I}{}_{acid})$ is the limiting value of $E_{1/2}$ at pH below pK_a. Using $n=1$, the fit gives access to an $E_{1/2}(Cu^{II/I}{}_{acid})$ of $+0.01\pm0.01$ V and a pK_a of 2.6 ± 0.1. This supports a monoelectronic proton-coupled electron process wherein reduction of Cu^{II} to Cu^{I} is accompanied by the protonation of the phenolate group. This assumption is further confirmed by the observation of an irreversible oxidation peak at $E_p=-0.1$ V at the foot of the Cu^{I} oxidation peak (Figure 1B). This oxidation process might correspond to the oxidation of a Cu^{I} species, which is formed by partial decoordination of the phenol moiety upon reduction of the Cu^{II} phenolate into Cu^{I} phenol according to an EC mechanism.[21] Notably, the pK_a value determined from the fit of Equation (1) is slightly lower than that measured spectrophotometrically in the DMF/water mixture, presumably owing to the absence of organic solvent and weak coordination of the buffer counter ions in the former case.

The functionalized MWCNT electrodes were then studied in the presence of oxygen (Figure 3).

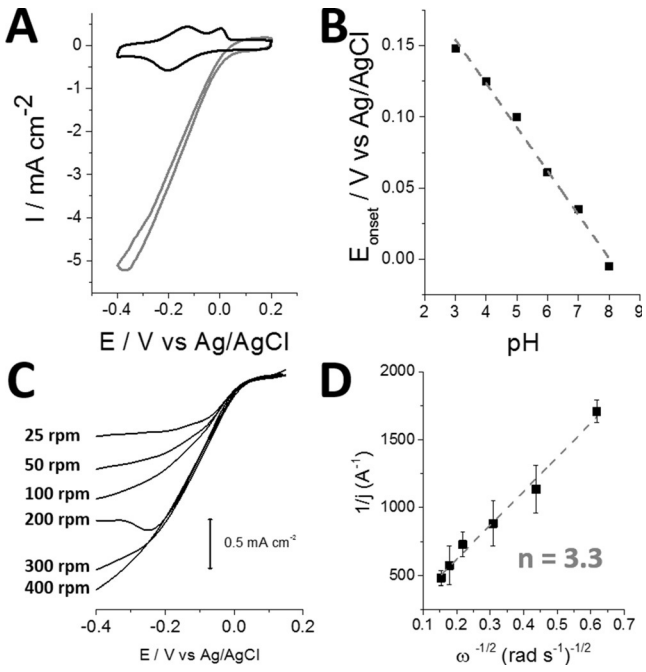

Figure 3. A) CVs of **1** immobilized on a MWCNT electrode in 0.1 M Britton–Robinson buffer at pH 5 under (black) argon and (gray) oxygen ($\nu=10$ mV s^{-1}); B) Evolution of the onset potential of the ORR as a function of the pH in 0.1 M Britton–Robinson buffer between pH 3 and 8. C) CV at the RDE between 25 and 400 rpm at pH 5 ($\nu=10$ mV s^{-1}); D) Associated Koutecky–Levich plot.

At oxygen saturation and continuous O_2 purging, an irreversible cathodic peak current was observed with an onset potential of $E_p^{red}=+0.10$ V versus Ag/AgCl at pH 5 (or $+0.60$ V vs. RHE), demonstrating their electrocatalytic activity towards ORR (Figure 3A). It is noteworthy that pristine MWCNTs also have an electrocatalytic activity towards ORR, but the onset potential is lower (0.03 V vs. Ag/AgCl at pH 5; Figure S9A). To unravel the catalytic pathway, the electrochemical behavior of the functionalized MWCNTs was investigated over a broad range of pH (Figure 3B). While the pH has little influence on maximum current densities between pH 3 and 8, a slope of 31 mV per pH unit was observed for the variation of onset potential towards pH. This is consistent with a $2e^-/1H^+$ limiting step for the electrocatalysis. The Tafel slope of around 70 mV per decade observed at pH 5 also confirms that the rate determining step involves a two electron process (Figure S9B). The rate-determining step, therefore, corresponds to the reduction of O_2 into a hydroperoxo species, similar to previously reported biomimetic catalysts.[7,8,19] Figure 3C and D display the rotating-disk experiments performed at pH 5. The diffusion-controlled electrocatalytic wave between 25 rpm and 400 rpm allowed for the calculation of the total number of electrons involved in the reaction. It is noteworthy that above 400 rpm, the electrocatalytic current density reaches a plateau, corresponding to kinetic limitations. By using the Koutecky–Levich equation, an apparent number of electrons of 3.3 ± 0.2 was estimated from independent measurements on several electrodes. Additionally, rotating-ring-disk electrode experiments were performed to detect H_2O_2. Consistent with an almost complete $4H^+/4e^-$ ORR process, no H_2O_2 generation could be evidenced within 0.1% (Figure S9C). This might also be caused by kinetic limitation observed for this complex at high rotating speed. Thus, the number of electrons measured between 3 and 4 is rather indicative of an efficient $2e^-$ reduction of oxygen into peroxide, followed by a slower $2e^-$ process, achieving the complete reduction of oxygen into water.[7] To validate this hypothesis, we examined the ability of the immobilized complex **1** to electrochemically reduce H_2O_2. The CV of the MWCNT-supported complex **1** performed in the presence of hydrogen peroxide confirms its electrocatalytic H_2O_2 reduction activity at similar overpotentials compared to the ORR (Figure S9D).

It is now instructive to compare the onset potential for oxygen reduction by MWCNT-supported **1** ($+0.60$ V vs. RHE) with values published for other immobilized copper complexes. It is close to the redox potentials observed for immobilized galactose oxidase ($+0.72$ V vs. RHE)[13] and some mononuclear copper complexes involving sterically hindered ligands immobilized in carbon black/nafion ink ($+0.60$ and $+0.67$ V vs. RHE),[22] but much lower than what was measured for dicopper catalysts based on (tris(2-pyridylmethyl)amine) ligands ($+0.86$ V vs. RHE) or reduced-graphene-oxide-supported multicopper/triazole-dipyridine complexes ($+0.95$ V).[23] This supports the involvement of a mononuclear species in the ORR in our case. In this sense, immobilized complex **1** acts as a galactose oxidase mimic by achieving the $2e^-/1H^+$ reduction of O_2 into a Cu^{II}-OOH intermediate,[3] but it is also able to achieve the reduction of

 © 2016 Wiley-VCH Verlag GmbH & Co. KGaA, Weinheim

H_2O_2 into H_2O, preventing release of hydrogen peroxide in solution. Finally, the kinetic performance of the MWCNT-supported complex **1** for ORR was evaluated. A substantial apparent turnover frequency (TOF) of 14 s^{-1} was determined at pH 5, based on the Γ_1 values determined above.

In conclusion, this work demonstrates the efficient and soft functionalization of MWCNT electrodes with a copper phenolato complex. We have established that the MWCNT-supported complex **1** achieves partial $4H^+/4e^-$ electrocatalytic reduction of dioxygen in a $2e^- + 2e^-$ reduction process. The reaction likely proceeds through formation of a Cu-OOH intermediate, which represents a bottleneck for efficient ORR. The rich redox chemistry of phenolate-based ligands brings new perspectives into the design of electrocatalysts inspired by the active site of galactose oxidase. Our future experiments will aim at modifying the ligand to decipher the role of the phenol moiety during catalysis, especially in the context of a proton-coupled electron transfer.

Acknowledgements

The authors wish to acknowledge the support from the platform Chimie NanoBio ICMG FR 2607 (PCN-ICMG) and from the LabEx ARCANE (ANR-11-LABX-0003-01).

Keywords: biomimetic chemistry · carbon nanotubes · copper · oxygen reduction · tripodal ligand

How to cite: *Angew. Chem. Int. Ed.* **2016**, *55*, 2517–2520
Angew. Chem. **2016**, *128*, 2563–2566

[1] E. A. Lewis, W. B. Tolman, *Chem. Rev.* **2004**, *104*, 1047–1076.
[2] E. I. Solomon, D. E. Heppner, E. M. Johnston, J. W. Ginsbach, J. Cirera, M. Qayyum, M. T. Kieber-Emmons, C. H. Kjaergaard, R. G. Hadt, L. Tian, *Chem. Rev.* **2014**, *114*, 3659–3853.
[3] J. W. Whittaker, *Chem. Rev.* **2003**, *103*, 2347–2364.
[4] D. Das, Y.-M. Lee, K. Ohkubo, W. Nam, K. D. Karlin, S. Fukuzumi, *J. Am. Chem. Soc.* **2013**, *135*, 2825–2834.
[5] S. Kakuda, R. L. Peterson, K. Ohkubo, K. D. Karlin, S. Fukuzumi, *J. Am. Chem. Soc.* **2013**, *135*, 6513–6522.
[6] C. C. L. McCrory, A. Devadoss, X. Ottenwaelder, R. D. Lowe, T. D. P. Stack, C. E. D. Chidsey, *J. Am. Chem. Soc.* **2011**, *133*, 3696–3699.
[7] E. C. M. Tse, D. Schilter, D. L. Gray, T. B. Rauchfuss, A. A. Gewirth, *Inorg. Chem.* **2014**, *53*, 8505–8516.
[8] M. A. Thorseth, C. E. Tornow, E. C. M. Tse, A. A. Gewirth, *Coord. Chem. Rev.* **2013**, *257*, 130–139.
[9] M. M. Whittaker, J. W. Whittaker, *J. Biol. Chem.* **1988**, *263*, 6074–6080.
[10] V. Soukharev, N. Mano, A. Heller, *J. Am. Chem. Soc.* **2004**, *126*, 8368–8369.
[11] C. F. Blanford, R. S. Heath, F. A. Armstrong, *Chem. Commun.* **2007**, 1710–1712.
[12] A. Le Goff, M. Holzinger, S. Cosnier, *Cell. Mol. Life Sci.* **2015**, *72*, 941–952.
[13] J. M. Abad, M. Gass, A. Bleloch, D. J. Schiffrin, *J. Am. Chem. Soc.* **2009**, *131*, 10229–10236.
[14] P. D. Tran, A. Le Goff, J. Heidkamp, B. Jousselme, N. Guillet, S. Palacin, H. Dau, M. Fontecave, V. Artero, *Angew. Chem. Int. Ed.* **2011**, *50*, 1371–1374; *Angew. Chem.* **2011**, *123*, 1407–1410.
[15] J. D. Blakemore, A. Gupta, J. J. Warren, B. S. Brunschwig, H. B. Gray, *J. Am. Chem. Soc.* **2013**, *135*, 18288–18291.
[16] P. Kang, S. Zhang, T. J. Meyer, M. Brookhart, *Angew. Chem. Int. Ed.* **2014**, *53*, 8709–8713; *Angew. Chem.* **2014**, *126*, 8853–8857.
[17] B. Reuillard, A. Le Goff, S. Cosnier, *Chem. Commun.* **2014**, *50*, 11731–11734.
[18] K. Ohara, M. Smietana, A. Restouin, S. Mollard, J.-P. Borg, Y. Collette, J.-J. Vasseur, *J. Med. Chem.* **2007**, *50*, 6465–6475.
[19] M. Orio, O. Jarjayes, H. Kanso, C. Philouze, F. Neese, F. Thomas, *Angew. Chem. Int. Ed.* **2010**, *49*, 4989–4992; *Angew. Chem.* **2010**, *122*, 5109–5112.
[20] E. Laviron, *J. Electroanal. Chem. Interfacial Electrochem.* **1979**, *101*, 19–28.
[21] This small irreversible redox oxidation is observed on the reversed scan after Cu^{II} reduction. Investigations at different scans and at different pH showed that the formation of this peak is favored at slow scan rates and low pH. Furthermore, a ratio of 1 for the sum of both anodic peaks over the cathodic peak suggest that the copper(II) phenolate species is regenerated upon this oxidation process. This is consistent with the protonation of the phenolate moiety upon reduction and further structural rearrangement of the reduced form of complex **1** in a favored trigonal or tetrahedral configuration of the Cu^{I}. This rearrangement is likely accompanied with the decoordination of the phenol moiety, this EC process being observed at the CV time scale by the presence of two anodic peaks.
[22] M. A. Thorseth, C. S. Letko, T. B. Rauchfuss, A. A. Gewirth, *Inorg. Chem.* **2011**, *50*, 6158–6162.
[23] Y.-T. Xi, P.-J. Wei, R.-C. Wang, J.-G. Liu, *Chem. Commun.* **2015**, *51*, 7455–7458.

Received: October 13, 2015
Revised: November 23, 2015
Published online: January 8, 2016

 © 2016 Wiley-VCH Verlag GmbH & Co. KGaA, Weinheim